Research Square

Preprints are preliminary reports that have not undergone peer review.
They should not be considered conclusive, used to inform clinical practice,
or referenced by the media as validated information.

Chemical Affinity-Controlled Element-Selective Heavy-Metal Immobilization Mechanism in Municipal Solid Waste Incineration Fly Ash-Asphalt Mastic

Yan Wang
Guangzhou North Second Ring Transportation Technology Co., Ltd
Xujia Zhou
Guangzhou North Second Ring Transportation Technology Co., Ltd
Ming Ye
Guangzhou North Second Ring Transportation Technology Co., Ltd
Yuanyu Lu
2112409097@mail2.gdut.edu.cn
Guangdong University of Technology
Xiaolong Sun
Guangdong University of Technology

Research Article

Keywords: MSWI fly ash, asphalt mastic, heavy metals, selective immobilization, chemical affinity

Posted Date: November 20th, 2026

DOI: https://doi.org/10.21203/rs.3.rs-11420654/v1

License: This work is licensed under a Creative Commons Attribution 4.0 International License.
Read Full License

Additional Declarations: No competing interests reported.

Chemical Affinity-Controlled Element-Selective Heavy-Metal Immobilization Mechanism in Municipal Solid Waste Incineration Fly Ash-Asphalt Mastic

Yan Wang[1], Xujia Zhou[1], Ming Ye[1], Yuanyu Lu[2*], Xiaolong Sun[2]

1. Guangzhou North Second Ring Transportation Technology Co., Ltd., Guangzhou, 510540, China

2. School of Civil and Transportation Engineering, Guangdong University of Technology, Guangzhou, 510006, China

Corresponding author: Yuanyu Lu, 2112409097@mail2.gdut.edu.cn

Abstract: To establish a multi-condition leaching monitoring scheme and clarify the environmental risk mechanism of municipal solid waste incineration (MSWI) fly ash reused as asphalt filler, seven heavy metals (Cr, Zn, Cu, Cd, Pb, Mn, Fe) were investigated through X-ray fluorescence (XRF) analysis, the European Community Bureau of Reference (BCR) sequential extraction, standard leaching tests, four service condition simulations (ultraviolet (UV) aging aging, high-temperature aging, spray, condensation), Fourier transform infrared (FTIR) characterization, and correlation analysis. The element-selective immobilization mechanism in fly ash–asphalt mastic was revealed from occurrence form, immobilization efficiency, environmental response, and chemical mechanism. Immobilization efficiency followed Cd (99.8%) > Zn (94.4%) > Pb (93.2%) > Cr (92.1%) > Cu (88.8%) > Mn (88.7%) > Fe (25.8%). Low Fe arose from intrinsic stability dominated by reducible and residual fractions, with limited asphalt immobilization. Environmental sensitivity under four conditions was Cd > Zn > Mn > (Cu/Pb) > Cr ≈ Fe, with Cd most sensitive. After UV aging, Cd leaching increased from 0.6 ppb to 1003.8 ppb (a 1673-fold increase), while Cr and Fe leaching were suppressed. Strong coordination between aging-generated polar functional groups and trivalent cations was the key driver. Ionic radius did not significantly correlate with immobilization efficiency ($r = 0.41$, $p > 0.05$). Two retardation mechanisms were proposed, and Cd and Zn were identified as priority pollutants for environmental risk control. The results can provide a quantitative basis for environmental risk monitoring and hierarchical management of MSWI fly ash recycling in pavement engineering.

Keywords: MSWI fly ash; asphalt mastic; heavy metals; selective immobilization; chemical affinity

Introduction

With the acceleration of urbanization, the generation of municipal solid waste in China has continued to rise. Incineration disposal, owing to significant advantages in volume reduction, harmlessness, and energy recovery, has become the mainstream technology for terminal treatment of municipal solid waste (Lu et al., 2020). However, fly ash produced as a by-product during waste incineration is enriched with multiple heavy metals such as Cr, Zn, Cu, Cd, and Pb as well as persistent organic pollutants, and exhibits prominent environmental toxicity. It has been explicitly classified as hazardous waste, and its safe disposal and large-scale consumption have become a core bottleneck constraining the sustainable development of the incineration industry (Ajorloo et al., 2022; Su et al., 2025). The chemical composition of municipal solid waste incineration (MSWI) fly ash is dominated by oxides such as CaO, SiO_2, and Al_2O_3, and it possesses physicochemical characteristics of fine particle size, well-developed pores, and large specific surface area, giving it natural technical adaptability as a filler to replace natural mineral materials in asphalt road engineering. Incorporating fly ash into asphalt systems can not only achieve resource utilization and consumption of large-volume hazardous waste and alleviate landfill site pressure, but also rely on the encapsulation barrier effect of asphalt binder to inhibit heavy metal leaching and release, representing an important technical pathway that balances environmental and economic benefits (Cho et al., 2020; Sun et al., 2025a). Existing studies have confirmed that fly ash-asphalt mastic and mixtures possess both good pavement mechanical performance and heavy metal immobilization capacity, providing a practical basis for road resource utilization of MSWI fly ash (Sun et al., 2023a; Yan et al., 2019).

However, it should be noted that the actual service environment of fly ash–asphalt mastic is complex and variable. Long-term actions of environmental factors such as UV irradiation, temperature fluctuation, rainfall scouring, and wet–dry alternation can easily induce aging degradation of the asphalt matrix and deterioration of interfacial structure, which not only damages the long-term service performance of pavement but may also disrupt the occurrence equilibrium of heavy metals in the fly ash–asphalt system, destroy the retardation barrier of asphalt, and lead to heavy metal dissolution and migration, posing a potential threat to the surrounding soil and groundwater ecological environment (Hazim et al., 2026; Sun et al., 2026a). This superimposed effect of performance attenuation and environmental risk is concealed

and lagging, making later treatment and remediation difficult and costly, and severely constraining the large-scale safe application of MSWI fly ash in road engineering (Ajorloo et al., 2022; Cho et al., 2020).

To enhance the heavy metal immobilization efficiency and environmental stability of fly ash–asphalt systems, researchers worldwide have conducted extensive research and achieved phased progress at three levels: material optimization, service condition response, and mechanism elucidation (Ajorloo et al., 2022; Sun et al., 2026b; Sun et al., 2025b). At the material optimization level, water washing pretreatment can effectively remove soluble salts and free heavy metals from fly ash, reducing heavy metal migration activity from the source. Asphalt modification and component regulation can further improve the retardation capacity of the asphalt matrix for heavy metals by strengthening physical encapsulation and interfacial adsorption (Sun et al., 2023b). At the service condition response level, existing studies have confirmed that single environmental factors such as high-temperature aging, ultraviolet (UV) aging, and water erosion can regulate heavy metal leaching behavior. Different environmental factors affect the release rate and extent of heavy metals by altering the structural integrity and chemical properties of asphalt(Wang et al., 2024a; Zou et al., 2023). At the mechanism elucidation level, the combined use of multiple characterization techniques such as X-ray fluorescence (XRF) spectrometry, inductively coupled plasma mass spectrometry (ICP-MS), and Fourier transform infrared (FTIR) spectroscopy has enabled multidimensional analysis from total element content and leachate concentration to functional group evolution, promoting the understanding of immobilization mechanisms from macroscopic phenomena to microscopic interactions (Sun et al., 2023b; Xu et al., 2024a).

Nevertheless, current research still has three obvious deficiencies. First, evaluations of heavy metal immobilization effects mostly use overall leaching amount as the core indicator, with insufficient attention to differences in immobilization efficiency among different elements, and there is a lack of systematic extraction and intrinsic cause analysis of element-selective immobilization patterns. Second, environmental impact studies are mostly conducted under a single service condition, lacking horizontal systematic comparison among multiple typical service conditions such as UV aging, high-temperature, spray, and condensation. The differences in environmental sensitivity among heavy metals remain unclear, and the regulatory weights of environmental factors and intrinsic element properties on leaching behavior need to be clarified. Third, explanations of immobilization mechanisms mostly focus on physical encapsulation and simple adsorption, and the deep scientific issues, including the evolution of polar functional groups during asphalt aging, coordination complexation between heavy metal ions and

functional groups, intrinsic mechanisms of differences in element chemical affinity, and the regulatory effect of occurrence form on immobilization efficiency, remain insufficiently revealed, making it difficult to support targeted environmental risk prevention and control and material optimization design (Hazim et al., 2026; Nan et al., 2026; Sun et al., 2025b; Yang et al., 2018; Zhang et al., 2024).

To address the above issues and establish an environmental risk assessment method for fly ash–asphalt systems, this study selected seven typical heavy metals in MSWI fly ash (Cr, Zn, Cu, Cd, Pb, Mn, Fe) as research objects, and carried out a systematic investigation covering occurrence form characterization, static immobilization efficiency quantification, multi-condition environmental response monitoring, and chemical mechanism elucidation. XRF elemental analysis and BCR sequential extraction procedure were used to clarify the initial occurrence characteristics of heavy metals in fly ash; standard leaching tests were used to quantify the immobilization efficiency of asphalt mastic for different elements; simulations of four typical service conditions, including UV aging, high-temperature, spray, and condensation, were used to reveal differences in environmental response among different elements; and FTIR characterization combined with correlation analysis was used to elucidate the regulatory mechanism of chemical affinity on selective immobilization, ultimately establishing differentiated heavy metal retardation modes based on intrinsic ionic properties. The research results can provide technical support for environmental risk monitoring, priority pollutant screening, and hierarchical risk assessment of MSWI fly ash used in road engineering, and are of great significance for promoting solid waste recycling and green low-carbon development of road engineering.

Raw Materials and Test Methods

Raw Materials

MSWI Fly Ash

MSWI fly ash from a waste incineration power plant in Dongguan was selected as the research object. It was a gray-black powder and easily absorbed moisture and agglomerated when exposed to air. The basic physical properties were tested according to the *Test Methods of Aggregate for Highway Engineering* (JTG 3432-2024, equivalent to the ASTM C series and EN 1097 series international standard systems for aggregate testing). The results showed that the specific surface area was 6.86 m^2/g,

the apparent density was 2.37 g/cm³, the pH was 12.09, and the particle size was mainly distributed in the range of 1–100 μm. The sample was screened through a 0.075 mm standard sieve and set aside for later use.

Asphalt Binder

70# base asphalt was selected as the carrier asphalt to prepare mastic. Its technical performance indicators were determined according to the Chinese Standard *Test Methods of Bitumen and Bituminous Mixtures for Highway Engineering* (JTG 3410-2025). This set of test methods was consistent in principle with and equivalent in core parameters to the internationally used ASTM D series, EN series, and ISO asphalt test standard systems. Its technical performance indicators are shown in Table 1.

Table 1 Performance indicators of 70# base asphalt

Test item	Test result	Technical requirement	Test specification
Penetration (25°C, 100 g, 5 s, 0.1 mm)	63.1	60-80	T0604-2025
Ductility (15°C, 5 cm/min)	>150	≥100	T0605-2025
Ductility (10°C, 5 cm/min)	20.3	≥20	T0605-2025
Softening point (ring-and-ball method, °C)	46.9	≥45	T0606-2025
Brookfield viscosity (135°C, mPa·s)	508.3	/	T0625-2011
Brookfield viscosity (175°C, mPa·s)	85.2	/	T0625-2011

Preparation of Fly Ash–Asphalt Mastic

Water washing pretreatment of fly ash: Fly ash and deionized water were weighed and mixed at a liquid-to-solid ratio of 8:1 (mass ratio). The mixture was stirred with a high-speed shear apparatus at 500 rpm for 10 min. After standing and settling for 30 min, the sediment was taken and dried in an oven at 105°C for 8 h. It was then screened through a 0.075 mm standard sieve to remove soluble salts and free impurities, obtaining pretreated fly ash. The water washing process of fly ash is specifically shown in Fig. 1.

Preparation of fly ash–asphalt mastic: The pretreated fly ash was placed in an oven at 160°C and dried for 4 h, and 70# base asphalt was heated in an oven at 160°C for 30 min. At a filler-binder ratio of 0.4 (mass ratio of fly ash to asphalt), the fly ash was added to the molten asphalt. The mixture was sheared

with a high-speed shear apparatus at 160°C and 2000 rpm for 10 min. After cooling to room temperature, a uniformly dispersed fly ash–asphalt mastic sample was obtained. The specific preparation process of fly ash–asphalt binder is shown in Fig. 1.

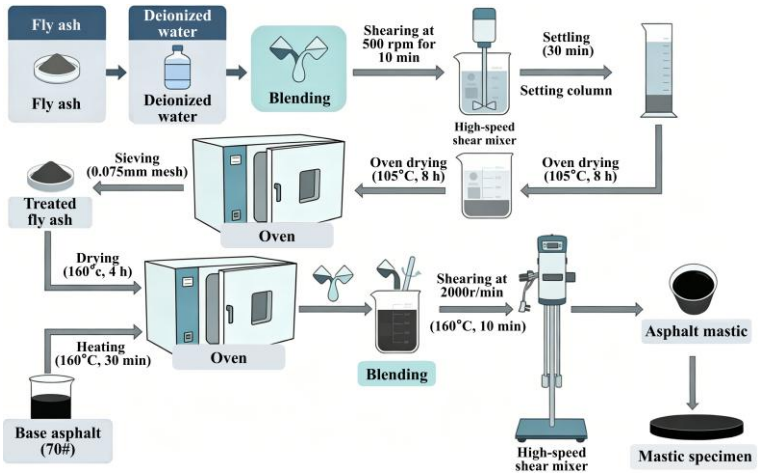


Fig. 1 Flowchart of fly ash water washing pretreatment and fly ash–asphalt mastic preparation

Heavy Metal Analysis Methods

Determination of Total Element Content by XRF

A Thermo Fisher ARL PERFORM'X 4200 wavelength-dispersive X-ray fluorescence (WDXRF) spectrometer was used for analysis. The excitation voltage was ≥70 kV, the excitation current was ≥140 mA, the analyzable element range was Be–U, and the concentration measurement range was ppm–100%. After the fly ash sample was dried at 105°C for 2 h to remove adsorbed water, particles passing through a 0.075 mm sieve were taken for powder pressing sample preparation. Each sample was tested in parallel three times, and the average value was taken.

BCR Sequential Extraction Procedure

The BCR three-step extraction procedure established by Rauret et al. (1999) (with an additional residual fraction digestion step) was used to divide the occurrence forms of heavy metals in fly ash and fly ash–asphalt mastic into four categories: (1) Acid-soluble fraction (F1): 50 mL of 0.11 mol/L acetic acid was added to 1 g of sample, and the mixture was subjected to reciprocating shaking at 22 ± 5°C for 16 h; (2) Reducible fraction (F2): 40 mL of 0.5 mol/L hydroxylamine hydrochloride solution (pH

adjusted to 1.5 with dilute nitric acid) was added to the F1 residue, and the mixture was shaken at room temperature for 16 h; (3) Oxidizable fraction (F3): 10 mL of 8.8 mol/L hydrogen peroxide was added to the F2 residue. After standing at room temperature for 1 h, the mixture was heated in a water bath at 85 ± 2°C to near dryness, and the operation was repeated once. After cooling, 50 mL of 1 mol/L ammonium acetate was added, and the mixture was shaken for 16 h; (4) Residual fraction (F4): the F3 residue was digested using a HCl-HNO_3-HF-$HClO_4$ high-pressure closed digestion method. The extract from each step was filtered through a 0.45 μm polyethersulfone membrane, and the heavy metal concentration was determined by ICP-MS. The BCR sequential extraction procedure is shown in Fig. 2.

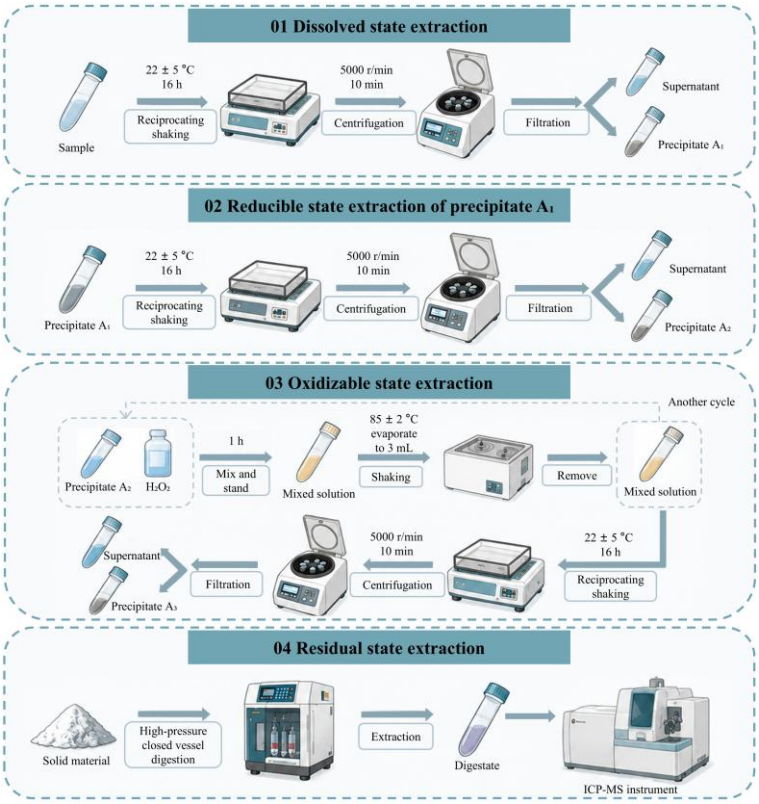


Fig. 2 Flowchart of BCR sequential extraction procedure for heavy metals in fly ash and fly ash–asphalt mastic

Standard Leaching Test

According to HJ/T 299-2007 *Solid Waste – Extraction Procedure for Leaching Toxicity – Sulfuric Acid-Nitric Acid Method*, concentrated sulfuric acid and concentrated nitric acid were mixed at a mass ratio of 2:1 and then added to deionized water, and the pH was adjusted to 3.20 ± 0.05. The original fly ash sample was directly used for leaching after sieving through a 0.075 mm sieve. The standard fly ash–asphalt mastic sample was first frozen at −5°C for 12 h according to the procedure in Fig. 3 and then

crushed at −5°C. The crushed sample (dry basis) and extraction liquid were placed in a 2 L polyethylene bottle at a liquid-to-solid ratio of 10:1 (mL/g). The bottle was shaken on a horizontal shaker at 110 oscillations/min for 8 h and then left to stand for 16 h. The supernatant was taken and filtered through a 0.45 μm filter membrane. The filtrate was diluted 100-fold with 1% nitric acid and then quantitatively analyzed using a Thermo Fisher iCAP RQ ICP-MS. Under standard mode, the detection limit for low-mass-number elements was ≤0.2 ppt (0.2 ng/L). Three parallel samples were set for each sample. The sample preparation procedure is shown in Fig. 3.

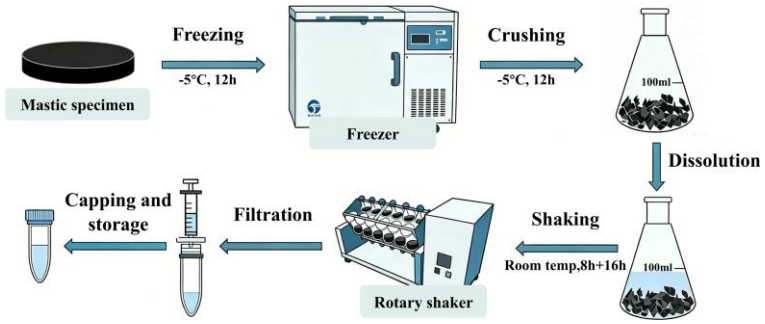


Fig. 3 Flowchart of sample preparation for leaching test of fly ash–asphalt mastic

Environmental Exposure Conditions

Light environment simulation: The light environment simulation centered on the UV aging test and was used to evaluate the individual effect of UV irradiation on the migration behavior of heavy metals in mastic. The test was conducted in a UV accelerated weathering test chamber. The distance between the UV lamps and the specimen surface was controlled at 35 cm, and the temperature inside the chamber was 60°C. Under these conditions, 1 day of UV aging simulation test was equivalent to 27 days of outdoor aging effect (taking Guangzhou as an example). According to the conversion relationship between indoor and outdoor aging time, the UV irradiation time was set to 330 h, corresponding to the equivalent aging degree of 12 months of outdoor exposure.

Temperature environment simulation: The temperature environment simulation was used to evaluate the individual effect of environmental temperature variation on the migration behavior of heavy metals in mastic. The test was conducted in a constant temperature test chamber. According to the normal-temperature, high-temperature, and extreme-high-temperature conditions actually experienced by pavement, the test temperature was set to 90°C, and the treatment time was 82.6 h to simulate the service duration of one quarter in summer.

Water environment simulation: The water environment simulation was used to evaluate the individual effects of humidity variation and rainfall scouring on the migration behavior of heavy metals in mastic. The test was divided into two independent modes: condensation (high humidity) and spray (scouring). In the condensation mode, the duration of a single humidity cycle was 4 h; in the spray mode, the duration of a single spray cycle was 12 min. Three cycles were set for each mode.

Specimen preparation: The molten MSWI fly ash–asphalt mastic was poured into a mold (diameter 28–29 mm, height 5 mm) to prepare standard specimens with a mass of (6.5 ± 0.2) g.

FTIR Spectroscopic Analysis

A Thermo Fisher Nicolet IS50 Fourier transform infrared spectrometer was used with attenuated total reflectance (ATR). Samples were directly scanned without pretreatment. The scanning range was 4000–450 cm^{-1}, the resolution was 4 cm^{-1}, and 32 scans were performed. Two parallel specimens were prepared for each sample, and each specimen was scanned twice. After scanning, the crystal plate was wiped with carbon disulfide solution to avoid cross-contamination. The characteristic functional group indices were calculated according to the following formulas:

$$\sum A = A_{-OH} + A_{C-H} + A_{C=O} + A_{S=O} \quad (1)$$

$$I_{-OH} = \frac{A_{-OH}}{\sum A} \quad (2)$$

$$I_{C-H} = \frac{A_{C-H}}{\sum A} \quad (3)$$

$$I_{C=O} = \frac{A_{C=O}}{\sum A} \quad (4)$$

$$I_{S=O} = \frac{A_{S=O}}{\sum A} \quad (5)$$

Where I_{-OH} is the hydroxyl functional group index; I_{C-H} is the alkane functional group index; $I_{C=O}$ is the carbonyl functional group index; $I_{S=O}$ is the sulfoxide group index; A_{-OH} is the absorption peak area in the range $[3700cm^{-1}, 3100cm^{-1}]$; A_{C-H} is the absorption peak area in the range $[3000\text{cm}^{-1}, 2750\text{cm}^{-1}]$; $A_{C=O}$ is the absorption peak area in the range $[1760\text{cm}^{-1}, 1530\text{cm}^{-1}]$; $A_{S=O}$ is the absorption peak area in the range $[1050\text{cm}^{-1}, 980\text{cm}^{-1}]$; and $\sum A$ is the sum of absorption peak areas in the range $[4000cm^{-1}, 450cm^{-1}]$.

Data Analysis Methods

Immobilization Efficiency (IE)

$$IE = \frac{C_{FA} - C_{Mastic}}{C_{FA}} \times 100\% \quad (6)$$

Where C_{FA} is the heavy metal leaching amount of the original fly ash (ppb), and C_{Mastic} is the heavy metal leaching amount of the fly ash–asphalt mastic (ppb). A higher IE value indicated a stronger static immobilization ability of asphalt for the element.

Environmental Sensitivity Index (ESI)

$$ESI = \frac{SD}{\bar{C}} \quad (7)$$

Where SD is the sample standard deviation of the leaching amount of an element under the four service conditions (ppb), and $\bar{C}$ is the arithmetic mean of the leaching amount under the four service conditions (ppb). ESI is a dimensionless parameter; the larger its value, the more sensitive the element is to environmental disturbance.

Correlation Analysis

To investigate the association between immobilization efficiency and intrinsic parameters, the Pearson correlation coefficient r was used for bivariate correlation analysis:

$$r = \frac{\sum_{i=1}^{n}(X_i - \bar{X})\,(Y_i - \bar{Y})}{\sqrt{\sum_{i=1}^{n}(X_i - \bar{X})^2} \cdot \sqrt{\sum_{i=1}^{n}(Y_i - \bar{Y})^2}} \quad (8)$$

Where X_i is the ionic radius (Shannon, 1976), and Y_i is the IE value of the corresponding element. The closer $|r|$ was to 1, the stronger the correlation. $|r| > 0.8$ was judged as strong correlation, $0.5 < |r| < 0.8$ as moderate correlation, and $|r| < 0.5$ as weak correlation.

Results and Discussion

Initial Occurrence Characteristics of Heavy Metals in Fly Ash

XRF Total Content Analysis

The total content analysis results of the seven heavy metals in fly ash are shown in Fig. 4. In terms of mass fraction, the element contents from high to low were: Zn (1.72 wt%), Fe (1.46 wt%), Pb (0.246 wt%), Cu (0.216 wt%), Mn (0.0528 wt%), Cr (0.0402 wt%), and Cd (0.0324 wt%). Zn and Fe together accounted for about 84.4% of the total amount of the seven heavy metals. The corresponding oxide contents were all higher than the element contents, such as ZnO at 2.14 wt%, Fe_2O_3 at 2.08 wt%, PbO at 0.265 wt%, CuO at 0.27 wt%, MnO at 0.0682 wt%, Cr_2O_3 at 0.0587 wt%, and CdO at 0.037 wt%. The higher oxide contents relative to elemental contents were attributed to the additional mass contributed by oxygen atoms in the oxide stoichiometry, which was consistent with the stoichiometric relationship.

Comparison of the XRF total content data with the standard leaching data showed that there was no corresponding relationship between element total content and leaching amount. Cr had a relatively low total content (0.0402 wt%), but its standard leaching amount was 3545 ppb, ranking first among the seven elements; Fe had the second highest total content (1.46 wt%), with a leaching amount of 2068 ppb, lower than that of Cr; Cd had the lowest total content (0.0324 wt%), with a leaching amount of 251 ppb. The inconsistency between the total content order and the leaching amount order suggested that the potential migration risk of heavy metals had no direct corresponding relationship with their absolute abundance in fly ash, but might be related to their occurrence chemical forms (Kang et al., 2025; Zhao et al., 2021).

It should be noted that the XRF total content was the mass fraction in the solid sample (wt%), the concentrations of BCR fractions were the mass concentrations in the corresponding extracts (ppb), and the standard leaching amount was the mass concentration in the leachate (ppb). The three had different bases and should not be directly compared numerically. The BCR results were mainly used to characterize the relative proportions of each fraction, and the standard leaching amount was used to evaluate migration risk.

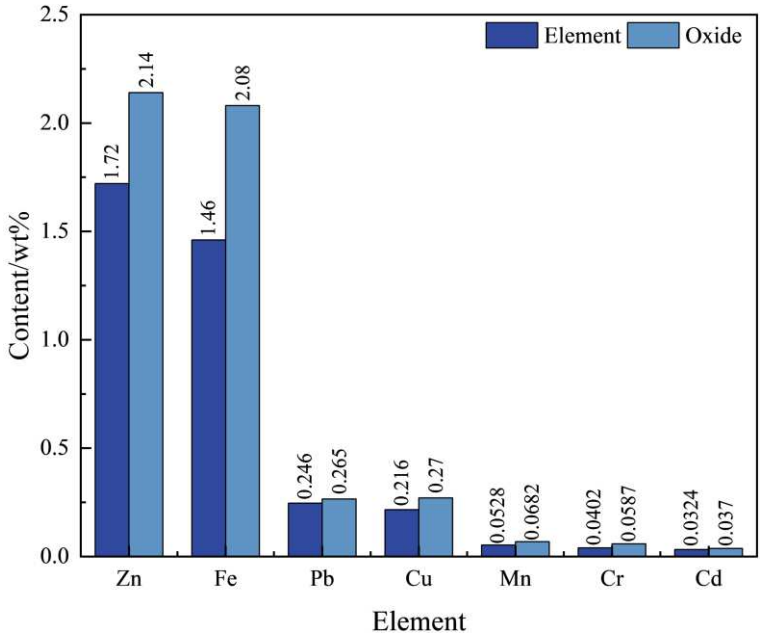


Fig. 4 Total element content by XRF

BCR Occurrence Form Distribution

The BCR sequential extraction results were expressed as the percentage of each fraction in the sum of the concentrations of the four extracts. The results are shown in Fig. 5. The occurrence form distribution of the seven elements could be classified into three types.

Acid-soluble fraction-dominated type (Cd, Zn). The occurrence form of Cd was absolutely dominated by the acid-soluble fraction, accounting for 81.29%, with the reducible fraction accounting for 16.51%, and the oxidizable and residual fractions accounting for 1.70% and 0.50%, respectively. The acid-soluble fraction of Zn accounted for 49.01%, the reducible fraction 26.54%, the oxidizable fraction 16.32%, and the residual fraction 8.13%. The high proportions of acid-soluble fraction for Cd and Zn indicated that they were mainly in exchangeable ion or carbonate-bound forms, which might be easily desorbed into the liquid phase when pH decreased or ionic strength changed. This indicated that the occurrence forms of Cd and Zn had relatively high potential migration risk (Pandey&Bhattacharya, 2019; Wu et al., 2020).

Reducible-residual fraction-dominated type (Fe). The occurrence forms of Fe were dominated by the reducible fraction (56.73%) and residual fraction (41.64%), with the acid-soluble fraction accounting for only 0.33% and the oxidizable fraction 1.30%. The high proportion of residual fraction for Fe might be attributed to the reaction of iron with other oxides at high temperature during incineration to form

mineral phases with stable lattice structures (such as Fe_2SiO_4, Fe_2O_3, Fe_3O_4), and such minerals had low dissolution rates in neutral to weakly alkaline environments (Zhang et al., 2022). The above occurrence distribution indicated that Fe had the highest intrinsic stability.

Mixed type (Cr, Pb, Cu, Mn). For Cr, the oxidizable fraction accounted for 58.43%, the residual fraction 35.00%, together accounting for 93.43%, the reducible fraction 5.42%, and the acid-soluble fraction only 1.15%. Pb was dominated by the reducible fraction (49.43%) and oxidizable fraction (35.62%). Cu was dominated by the reducible fraction (50.89%). Mn was dominated by the reducible fraction (53.16%) and acid-soluble fraction (28.68%). The occurrence distributions of the above elements were between those of Cd/Zn and Fe, and their environmental sensitivity also showed transitional characteristics (He&Kasina, 2023).

The BCR results indicated that Cd and Zn differed essentially from Cr and Fe in initial occurrence forms: the former were dominated by unstable forms with higher chemical activity, while the latter were dominated by stable forms with higher chemical inertness. This difference might provide a basis for explaining the element-selective immobilization and environmental sensitivity order of asphalt mastic later (Nag et al., 2020).

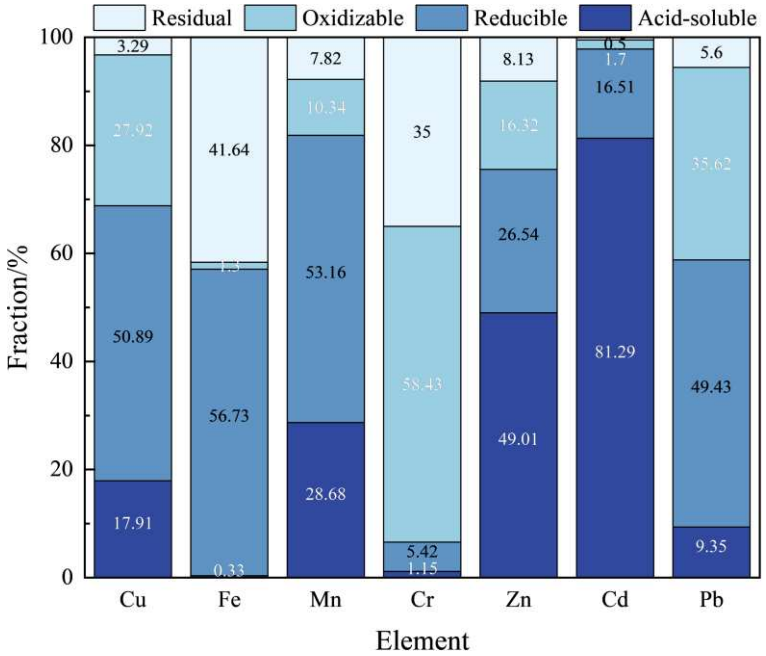


Fig. 5 BCR occurrence form distribution

Control of Occurrence Form on Leaching Behavior

To comprehensively characterize the relationship among total content, occurrence form, and

leaching behavior, Fig. 6 used the sum of the concentrations of the four BCR extracts as the horizontal axis, the standard leachate concentration as the vertical axis, and the proportion of acid-soluble fraction as the color mapping to show the differences in leaching behavior of the seven heavy metals. The Cr point was close to the y = x reference line, indicating that its leaching amount was close to the extraction amount corresponding to the BCR extract concentration; the Zn and Fe points were far below the reference line, indicating that although their BCR extraction amounts were high, their release amounts were limited; the Cd point had the warmest color, corresponding to the highest proportion of acid-soluble fraction, suggesting a relatively high potential migration risk.

Combined with the aforementioned BCR occurrence form distribution, it could be seen that Cd and Zn had high proportions of acid-soluble fraction, so although Cd had the lowest total content, its leaching risk was the highest; Cr and Fe had high proportions of stable forms, so although Cr had a relatively low total content and Fe had a relatively high total content, their leaching amounts did not change synchronously with the total content. The above results further indicated that the leaching behavior of heavy metals might be dominated by their occurrence forms rather than total amount, and occurrence form was the primary intrinsic factor controlling migration risk. This conclusion provided a basis for explaining the element-selective immobilization and environmental sensitivity order of asphalt mastic later (He et al., 2023; Long et al., 2022).

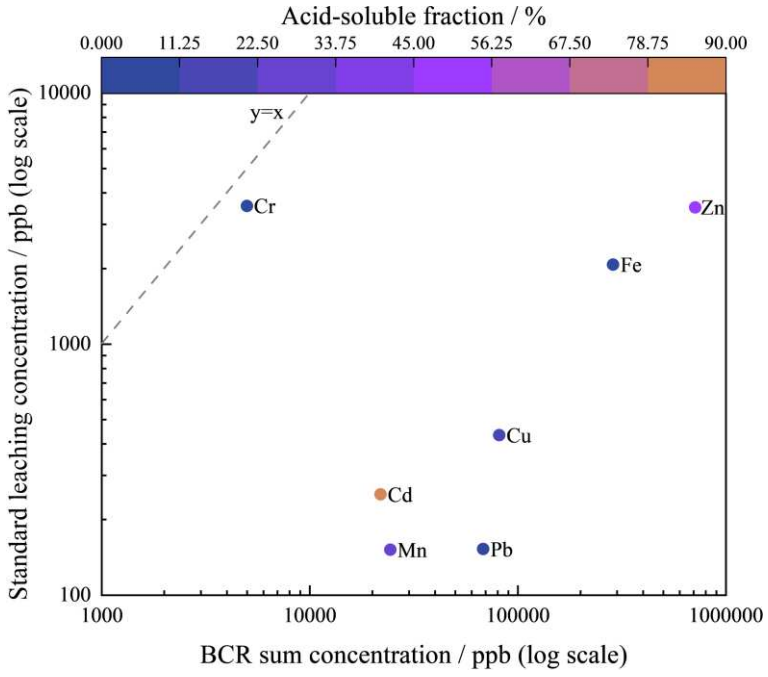


Fig. 6 Comparison between total BCR extraction concentration and standard leaching concentration

Element-Selective Immobilization of Asphalt Mastic

Leaching Comparison of Elements under Standard Leaching Conditions

After fly ash was compounded with asphalt, the leaching results under standard HJ/T299-2007 conditions are shown in Fig. 7(a). The leaching amounts of all elements decreased to varying degrees: Cd decreased from 251 ppb to 0.6 ppb, Zn from 3498 ppb to 196.2 ppb, Pb from 152 ppb to 10.4 ppb, Cr from 3545 ppb to 280.6 ppb, Cu from 432 ppb to 48.5 ppb, Mn from 151 ppb to 17.1 ppb, and Fe from 2068 ppb to 1533.6 ppb. The decreases differed significantly among elements. The leaching amount of Cd decreased to about 1/418 of the initial value, with a decrease of 99.8%; the leaching amount of Fe decreased to about 1/1.35 of the initial value, with a decrease of 25.8%.

It is noteworthy that the decrease of Fe (25.8%) was much lower than that of other elements (all >88%). This might not be due to insufficient immobilization capacity of asphalt for Fe, but because Fe mainly occurred in reducible (56.73%) and residual (41.64%) fractions in fly ash, which together accounted for 98.37%, and its intrinsic migration activity was extremely low (the leaching rate of original fly ash was only 0.72%), so the marginal immobilization contribution of asphalt was naturally limited (Li et al., 2022; Sun et al., 2026c). In Fig. 7(a), the difference in the heights of the two bars for Fe was obviously smaller than that for other elements, intuitively reflecting this intrinsic stability.

Order of Immobilization Efficiency

The immobilization efficiency (IE) of each element was calculated according to Eq. (1), and the results are shown in Fig. 7(b). The IE of the seven elements from high to low was: Cd (99.8%), Zn (94.4%), Pb (93.2%), Cr (92.1%), Cu (88.8%), Mn (88.7%), and Fe (25.8%). Among them, the IE value of Fe was 25.8%, which differed from other elements by more than 63 percentage points and was an obvious outlier. In Fig. 7(b), the bar height of Fe was obviously lower than that of other elements and was marked in orange as an "outlier".

As mentioned above, the low IE value of Fe mainly originated from its low intrinsic migration activity and the limited marginal immobilization contribution of asphalt, rather than insufficient immobilization capacity of asphalt for Fe. Therefore, the low IE value of Fe was not contradictory to its high intrinsic stability, but was consistent with the core viewpoint that "occurrence form determines

leaching behavior" (Azadgoleh et al., 2022).

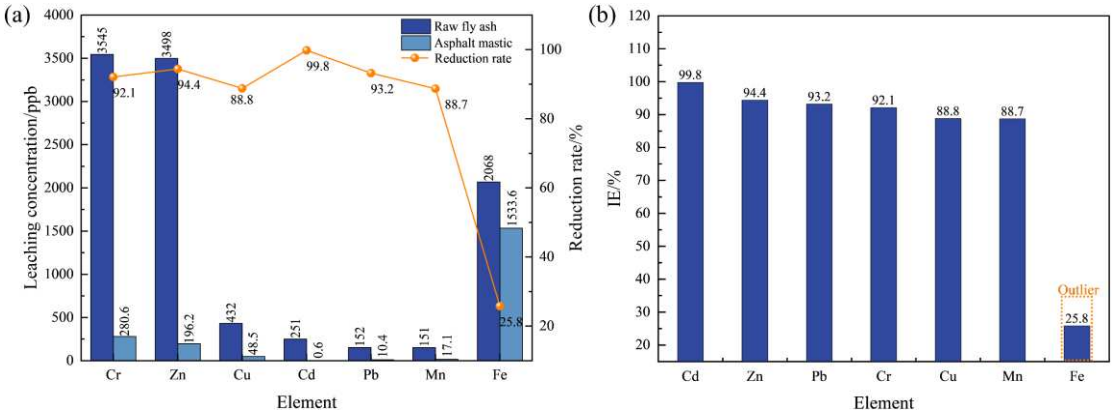


Fig. 7 Immobilization performance of asphalt mastic: (a) Comparison of leaching concentrations; (b) Order of immobilization efficiency (IE)

Relationship between IE and Environmental Sensitivity

IE characterizes the physical encapsulation efficiency of asphalt in the unaged state, but its value had no direct correspondence with the environmental stability of the material during long-term service. Cd had the highest IE (99.8%), but as will be demonstrated in the following analysis of environmental responses, Cd showed the largest increase in leaching under environmental disturbance; Fe had the lowest IE (25.8%), but its leaching amount decreased rather than increased under environmental disturbance. This comparison indicated that the IE value under standard leaching conditions alone might not fully evaluate the long-term immobilization effect of asphalt on heavy metals, and environmental sensitivity analysis should be combined (Zou et al., 2024). The next section will discuss the differentiated responses of different elements under environmental disturbance from four typical service conditions.

Differences in Environmental Sensitivity of Heavy Metals

Leaching Response under UV Aging Condition

The leachate concentrations of each element under the standard condition and four service conditions are shown in Fig. 8, and the fold changes relative to the standard condition are shown in Fig. 9. Under UV aging (330 h, 60°C), Cd increased from 0.6 ppb to 1003.8 ppb, corresponding to a 1673-fold increase relative to the unaged baseline; Zn increased from 196.2 ppb to 20028.3 ppb (~102-fold); Mn, Cu, and Pb all exhibited increasing trends, corresponding to ~43-fold, 1.35-fold, and 1.45-fold

increases, respectively. Cr decreased from 280.6 ppb to 218.7 ppb, a decrease of 22%; Fe decreased from 1533.6 ppb to 187.0 ppb, a decrease of 88%.

The effect of UV aging on heavy metal leaching might involve two competing mechanisms. First, UV radiation induced free-radical chain oxidation reactions of asphalt molecular chains, leading to volatilization of light components and the appearance of microcracks in the physical encapsulation structure, providing channels for heavy metal ion migration (Sun et al., 2026a; Zou et al., 2022). Second, photo-oxidation reactions introduced oxygen-containing polar functional groups (—OH, —C=O, —S=O) onto asphalt molecular chains, and these groups could act as ligands to complex with free metal ions (Wang et al., 2024b; Yang et al., 2023). The net balance of the two effects might determine the leaching direction of a specific element: for divalent cations such as Cd and Zn, the physical destruction effect might dominate, with a net increase in leaching amount; for trivalent cations such as Cr and Fe, the chemical complexation effect might be sufficient to offset the physical destruction effect, with a net inhibition of leaching. In Fig. 9, the cells for Cd and Zn were darker purple, and those for Cr and Fe were lighter blue, intuitively showing this differentiation.

Leaching Response under High-temperature Aging Condition

Under high-temperature aging (90°C, 82.6 h), the leachate concentration changes for each element are shown in Fig. 8 and Fig. 9. Cd increased from 0.6 ppb to 1657.1 ppb (a 2762-fold increase relative to the unaged baseline); Zn increased from 196.2 ppb to 17999 ppb (~92-fold); Mn, Cu, and Pb all exhibited increasing trends, corresponding to ~44-fold, 3.19-fold, and 1.34-fold increases, respectively. Cr decreased from 280.6 ppb to 178.1 ppb, a decrease of 37%; Fe decreased from 1533.6 ppb to 266.0 ppb, a decrease of 83%.

High-temperature aging exerted the strongest driving effect on metal leaching among the four environmental factors. Its mechanism might involve two aspects: first, high-temperature reduced asphalt viscosity and intensified molecular thermal motion, accelerating the diffusion rate of heavy metal ions from the surface of fly ash particles; second, high-temperature accelerated asphalt oxidation and increased the generation rate of polar functional groups, and the complexation immobilization effect on Cr^{3+} and Fe^{3+} might be more sufficient (Qu et al., 2026; Xu et al., 2024b; Zhao et al., 2019). The physical effect might dominate for most elements, so the leaching amount increased with increasing temperature.

In Fig. 9, the color block of Cd in the high-temperature column was the deepest purple in the entire figure, indicating that Cd had the highest risk under high-temperature.

Leaching Response under Water Environment Conditions

Under spray scouring (12 min/cycle, 3 cycles) and condensation high humidity (4 h/cycle, 3 cycles), the changes in leachate concentrations of the elements are shown in Fig. 8 and Fig. 9. Under the spray condition, Cd increased from 0.6 ppb to 993.9 ppb (~1657-fold), and Zn increased from 196.2 ppb to 17539.6 ppb (~88-fold); under the condensation condition, Cd increased from 0.6 ppb to 681.3 ppb (~1136-fold), and Zn increased from 196.2 ppb to 12821 ppb (~65-fold). Mn, Cu, and Pb were at a moderate sensitivity level under both water environment modes, and Cu under the condensation condition was even lower than under the standard condition. Cr and Fe remained inhibited under both water environment modes: under the spray condition, Cr decreased to 212.3 ppb and Fe to 236.8 ppb; under the condensation condition, Cr decreased to 226.6 ppb and Fe to 319.4 ppb.

The driving effect of the water environment on leaching might center on physical interface destruction. Water molecules penetrated along the asphalt–fly ash interface, formed a water film, weakened interfacial adhesion strength, and led to interfacial debonding and microcrack propagation; the spray mode additionally imposed a mechanical scouring effect on this basis (Hu et al., 2020; Zhao&Zhu, 2019; Zhou et al., 2024). For Cd, Zn, and Cu dominated by physical encapsulation, the leaching amount under the spray condition was higher than that under the condensation condition; however, Cr, Fe, and Pb did not show spray > condensation. Cr and Fe remained inhibited under both water environment modes, further supporting the cross-condition stability of the binding between trivalent cations and polar functional groups. In Fig. 9, both rows of the water environment showed a pattern of "Cd/Zn tending to purple, Cr/Fe tending to blue", consistent with the UV and high-temperature conditions.

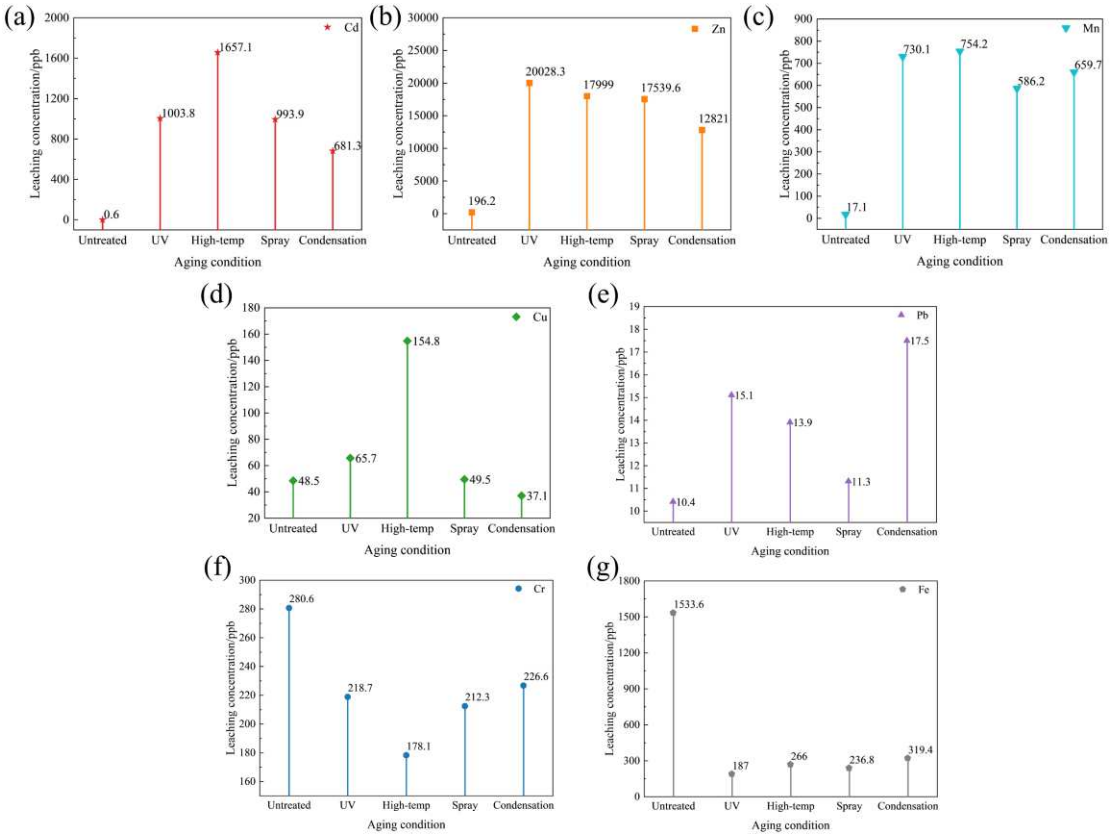


Fig. 8 Absolute leaching concentrations of seven heavy metals under different service conditions: (a) Cd, (b) Zn, (c) Mn, (d) Cu, (e) Pb, (f) Cr, (g) Fe

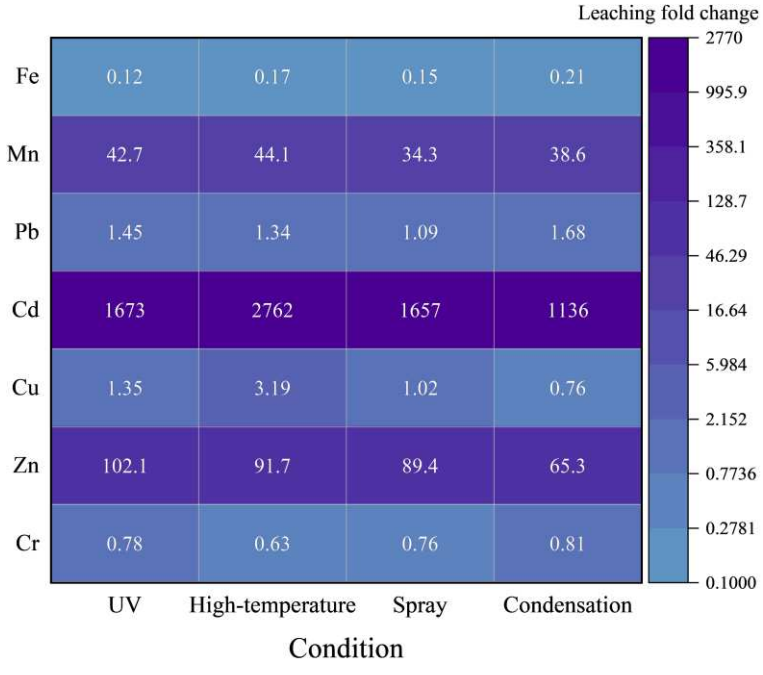


Fig. 9 Heatmap of leaching fold changes under four service conditions

Cross-Condition Sensitivity Order and Environmental Sensitivity Index

The leaching increases of each element under the four service conditions were ranked. The results showed that under all four conditions, Cd, Zn, and Mn were at the top, while Cr and Fe were at the lowest level; the order of Cu and Pb exchanged under different conditions, but both were generally in the moderate sensitivity range. The overall sensitivity order could be summarized as: Cd > Zn > Mn > (Cu/Pb) > Cr ≈ Fe. In the heatmap of Fig. 9, the rows for Cd, Zn, and Mn were more purple, and the rows for Cr and Fe were more blue, intuitively presenting the intrinsic differentiation of sensitivity among elements.

The consistency of the sensitivity order under the four service conditions has important mechanistic implications. The action mechanisms of the four environmental factors—UV, high-temperature, condensation, and spray—are essentially different: UV radiation is dominated by photon excitation and free radical oxidation, high-temperature by thermal activation and thermal-oxidative degradation, and the water environment by interfacial penetration and hydration stripping. If the type of environmental factor were the dominant controlling factor of leaching behavior, different action mechanisms should correspond to different element sensitivity orders. However, in terms of leaching fold, Cd, Zn, and Mn were always at the top, and Cr and Fe were always at the lowest level; the leaching folds of Cu and Pb were relatively low, and the fold of Cu under the condensation condition was only 0.76, lower than under the standard condition, showing inhibition characteristics similar to those of Cr and Fe. This phenomenon suggested that the primary factor determining the leaching sensitivity of heavy metals might be the intrinsic chemical properties of the elements rather than the type of external environmental factor. The role of environmental factors might be to regulate the triggering and intensity of leaching events, but could not change the inherent sensitivity hierarchy among different elements (Sun et al., 2026a).

The ESI values of each element were calculated according to Eq. (2), and the results are shown in Fig. 10. The ESI value of Cd was 0.38, Zn 0.18, Mn 0.11, Pb 0.18, Cr 0.10, Cu 0.69, and Fe 0.22. The ESI value of Cd was about 3.8 times that of Cr and about 2.1 times that of Zn. Fig. 10 shows the ESI of the seven elements using a horizontal dot plot and classified color bands: Cd and Zn fell in the high sensitivity zone, Mn and Pb in the medium-low sensitivity zone, and Cr in the insensitive zone. It should be noted that although the ESI value of Cu was high (0.69), its absolute increase fold was only 0.76–3.19 times, so its actual environmental risk might be limited; Fe was a negatively sensitive element, and its

ESI reflected the fluctuation of the decrease extent, which had a different meaning from that of positively sensitive elements. Overall, the ESI can be used as a quantitative indicator for long-term environmental risk monitoring and evaluation of fly ash–asphalt materials. Cd and Zn should be listed as priority targets for environmental safety prevention and control; although Cu had a relatively high ESI, its absolute leaching amount was limited, and its environmental risk should be judged comprehensively in combination with absolute concentration. The above results suggested that the environmental sensitivity order of heavy metals might be determined by their intrinsic chemical properties rather than the type of external environmental factor (Wekpe et al., 2024).

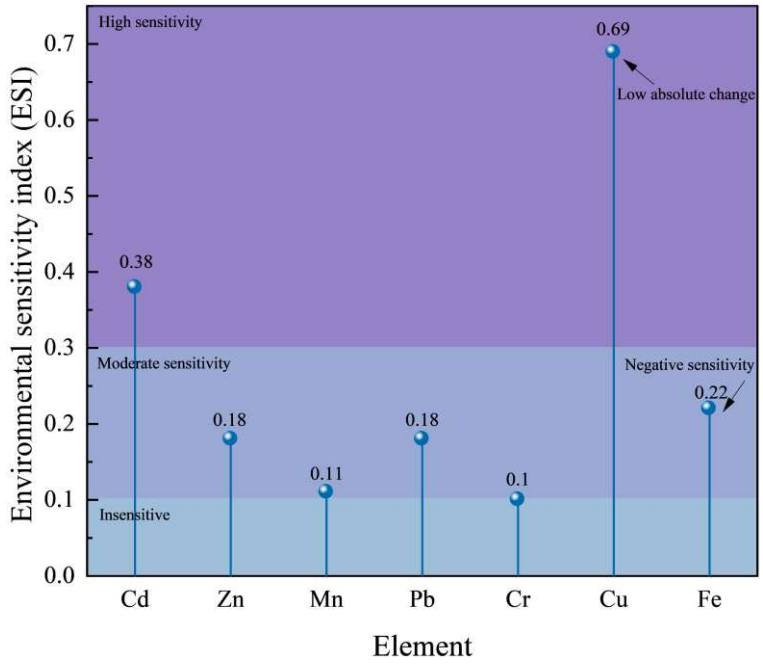


Fig. 10 Distribution of environmental sensitivity index (ESI)

Chemical Mechanism: Chemical Affinity Controls Migration Behavior

Correlation Analysis between Intrinsic Parameters and Immobilization Efficiency

Pearson correlation analysis was performed between IE and ionic radius. The correlation is shown in Fig. 11. The ionic radius data (six-coordination): Cd^{2+} (0.095 nm), Zn^{2+} (0.074 nm), Pb^{2+} (0.119 nm), Cr^{3+} (0.062 nm), Cu^{2+} (0.073 nm), Mn^{2+} (0.083 nm), Fe^{3+} (0.065 nm). The correlation coefficient between IE and ionic radius was $r = 0.41$ ($p > 0.05$), indicating no significant linear relationship between them. Ionic radius could only explain 16.7% of the IE variation ($R^2 = 0.167$). This result ruled out the possibility of ionic spatial size as the main controlling factor, indicating that element-selective immobilization was

more likely governed by the combined regulation of ionic valence and coordination chemistry (Florez et al., 2024; Grasseschi et al., 2020).

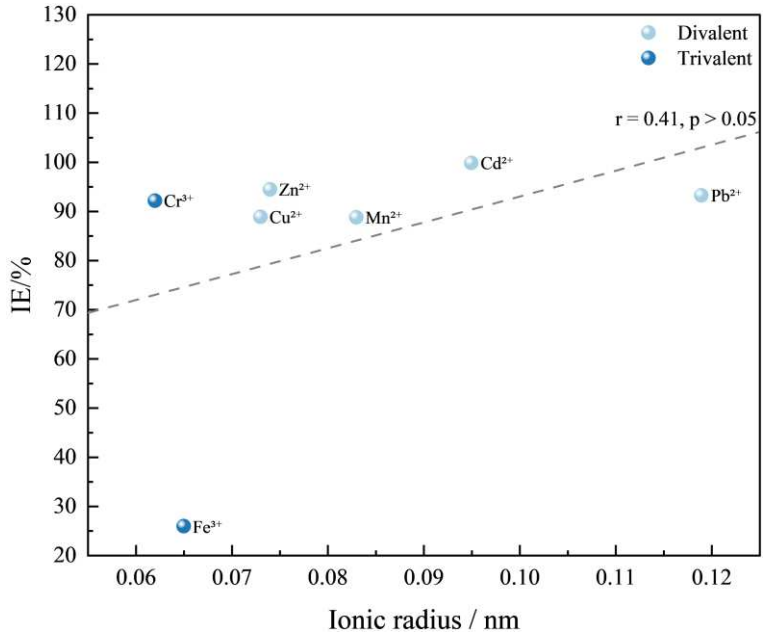


Fig. 11 Correlation between ionic radius and immobilization efficiency

Evolution of Polar Functional Groups during Aging

The FTIR spectra (Fig. 12) showed that the characteristic absorption bands of the untreated mastic appeared at 3396, 2919, 2850, and 1626 cm^{-1}, corresponding to hydroxyl (-OH) stretching vibration, aliphatic C-H stretching vibration, and carbonyl (C=O) stretching vibration, respectively. After aging under different conditions, the positions and intensities of the characteristic peaks changed to varying degrees. Under the UV 330 h condition, the -OH peak shifted from 3396 cm^{-1} for the untreated sample to 3421 cm^{-1} toward higher wavenumber, the C=O peak shifted from 1626 cm^{-1} to 1575 cm^{-1} toward lower wavenumber, and the absorption peak area of the sulfoxide group at 1031 cm^{-1} increased with increasing aging time. Under the high-temperature 90°C condition, the -OH peak shifted to 3403 cm^{-1}, the carbonyl-related absorption peak at 1605 cm^{-1} was enhanced, the absorption of oxygen-containing functional groups near 1154 and 1113 cm^{-1} was enhanced, and the sulfoxide peak area at 1031 cm^{-1} increased with increasing aging temperature. Under the spray-III and condensation-III conditions, the absorption peaks and functional group compositions in the spray and condensation environments were basically similar. The -OH peak at 3395 cm^{-1} gradually increased with the aging process, and the C=O peak at 1605 cm^{-1} formed a full peak shape. The above peak shifts and

intensity changes suggested that oxidation reactions occurred in asphalt molecular chains during aging, generating oxygen-containing polar functional groups such as hydroxyl, carbonyl, and sulfoxide groups. These polar functional groups might provide coordination sites for heavy metal ions, thereby affecting the migration behavior of heavy metals (Cui&Wang, 2023; Wang et al., 2024c; Xi et al., 2026; Xu et al., 2024c) .

To further quantify the changes in the above functional groups, peak area integration was performed on the FTIR spectra, and the functional group indices were calculated (Fig. 13). The results showed that after treatment under each environmental condition, the absorption peak areas and corresponding indices of the three functional groups (hydroxyl, carbonyl, and sulfoxide) in the asphalt mastic showed increasing trends. Under the UV aging condition, as the irradiation time increased from 0 h to 330 h, the hydroxyl index increased from 0.24 to 0.306, and the sulfoxide index increased from 0.001 to 0.030. Under the high-temperature condition (90°C), the hydroxyl index and carbonyl index reached 0.424 and 0.101, respectively, higher than those in the later stage of UV aging. Under the water environment conditions, the hydroxyl index increased significantly (0.480 for spray and 0.481 for condensation). In Fig. 13, the variation trends of the three functional group indices with aging conditions were clearly visible. Hydroxyl and carbonyl generally showed upward trends, and sulfoxide increased particularly obviously under UV and high-temperature.

The accumulation of polar functional groups during aging might have dual effects on heavy metal ions: (1) oxidation reactions led to chain scission and embrittlement of asphalt molecular chains, and the compactness of the physical encapsulation structure decreased; (2) newly formed polar groups acted as coordination sites and complexed with free heavy metal ions. The net leaching direction of a specific element might depend on the relative strength of the above two effects. For Cr^{3+} and Fe^{3+}, the complexation immobilization effect might dominate; for Cd^{2+} and Zn^{2+}, the physical destruction effect might dominate (Li et al., 2021; Zhao et al., 2023a; Zhong et al., 2026). This mechanism is further elaborated from the perspective of ionic valence in the next subsection.

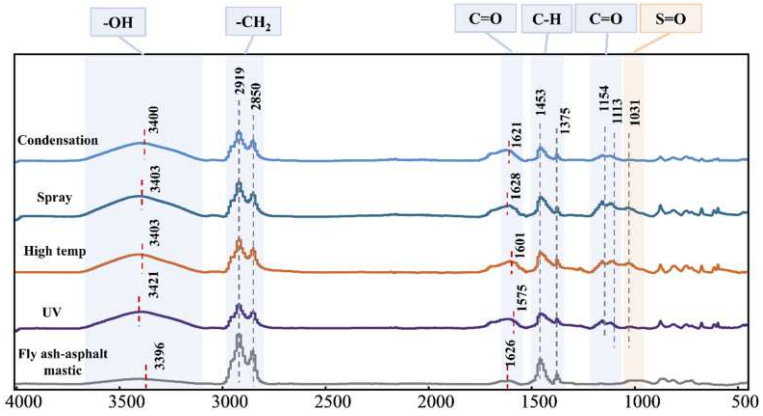


Fig. 12 Overlaid FTIR spectra under different aging conditions

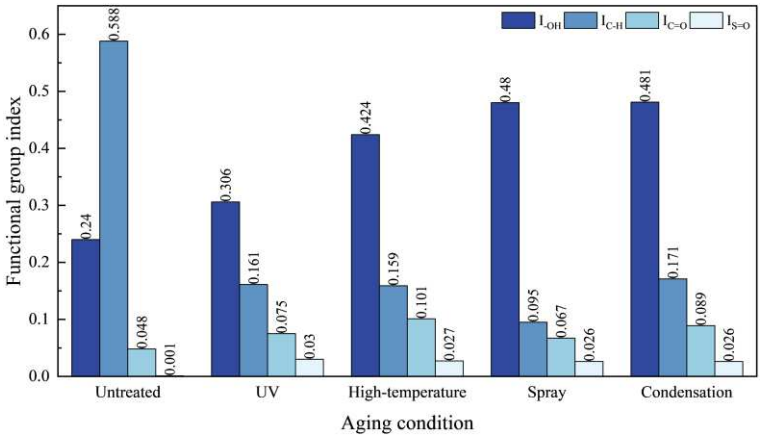


Fig. 13 Variation of each functional group index

Ionic Valence and Coordination Chemistry

The stable forms of Cr and Fe in the system were Cr^{3+} and Fe^{3+}, respectively. The charge densities of the trivalent cations were 48.4 e^{-}/nm for Cr^{3+} and 46.2 e^{-}/nm for Fe^{3+}. The stable forms of Cd and Zn were Cd^{2+} and Zn^{2+}, respectively, with charge densities of 21.1 e^{-}/nm and 27.0 e^{-}/nm. The charge densities of trivalent ions were about 1.7–2.3 times those of divalent ions. This difference might be one of the reasons leading to the differentiation in environmental sensitivity between the two types of elements (Bensiradj et al., 2026; Liu et al., 2019)

According to literature reports, the difference in charge density can be reflected in the complexation stability constant. The complexation stability constant of Fe^{3+} with carboxyl groups was on the order of 10^{10}, and that of Zn^{2+} with carboxyl groups was on the order of 10^{5}, differing by about 5 orders of magnitude. The complexation stability constant of Cr^{3+} was on the same order as that of Fe^{3+}, and Cd^{2+} and Zn^{2+} were on the same order. This difference suggested that in the presence of polar functional groups

at the same concentration, the tendency of trivalent ions to be complexed and immobilized might be much higher than that of divalent ions (Mohan et al., 2026; Xia et al., 2022; Zhao et al., 2023b).

For Cr^{3+} and Fe^{3+}, even if the physical structure of asphalt deteriorated due to aging, the polar groups generated during aging might still capture and immobilize them through relatively strong coordination bonds. The phenomenon that the leaching amount of Fe decreased rather than increased after UV and high-temperature aging might be related to the complexation immobilization effect exceeding the release effect caused by physical structure destruction in terms of magnitude (Sun et al., 2026a). For Cd^{2+} and Zn^{2+}, their coordination bonds with polar functional groups might be weaker and could not provide effective secondary immobilization under environmental disturbance, and the immobilization effect might mainly depend on the integrity of the physical encapsulation structure (Liu et al., 2021). This mechanism was consistent with the cross-condition pattern in Fig. 9 in which Cr and Fe were blue under all conditions, while Cd and Zn were purple.

Differentiated Retardation Mechanisms

Taken together, the foregoing results covering occurrence form characterization, immobilization efficiency quantification, environmental response analysis, and chemical mechanism elucidation demonstrate that the migration behavior of the seven heavy metals in fly ash-asphalt mastic can be summarized into two differentiated retardation modes based on ionic valence.

Chemical complexation-dominated type (Cr, Fe). These elements were mainly in stable forms in fly ash (residual + oxidizable fractions accounted for 93.43% for Cr, and reducible + residual fractions accounted for 98.37% for Fe) and existed as trivalent cations. The relatively high charge density might endow them with stronger coordination ability, forming relatively stable complexes with polar functional groups in asphalt (Cao et al., 2025; Xue et al., 2020). Under environmental disturbance, their leaching amounts did not increase but decreased or remained stable, with the lowest ESI values (Cr 0.10, Fe 0.22). In Fig. 10, Cr and Fe were located in the insensitive/negatively sensitive zone, consistent with this mechanism.

Physical encapsulation-dominated type (Cd, Zn). These elements were mainly in the acid-soluble fraction in fly ash (Cd 81.29%, Zn 49.01%) and existed as divalent cations. The relatively low charge density might lead to their coordination stability being significantly lower than that of trivalent ions, and

the immobilization effect mainly depended on physical encapsulation (Song et al., 2024; Sun et al., 2026c). Under environmental disturbance, their leaching amounts increased by orders of magnitude. The ESI values were 0.38 for Cd and 0.18 for Zn, which were relatively high among the physical encapsulation-dominated elements. In Fig. 10, Cd was located in the high sensitivity zone and Zn in the moderate sensitivity zone, consistent with this mechanism.

The occurrence forms and response characteristics of Pb, Cu, and Mn were between the above two types, showing transitional characteristics. Among them, although the ESI of Cu was high, its absolute increase was limited; the sensitivity levels of Mn and Pb were at a moderately low level. The above differentiated retardation mechanisms suggested that the immobilization of heavy metals by asphalt was not a single physical encapsulation process, but a synergistic result of chemical complexation and physical encapsulation, and its dominant mode was determined by the intrinsic properties of the elements (occurrence form, ionic valence, and charge density) rather than external environmental conditions. This mechanism can guide the targeted screening of monitoring indicators and the formulation of classified risk control strategies in practical engineering environmental monitoring (Song et al., 2024).

The overall mechanism is summarized in Fig. 14.

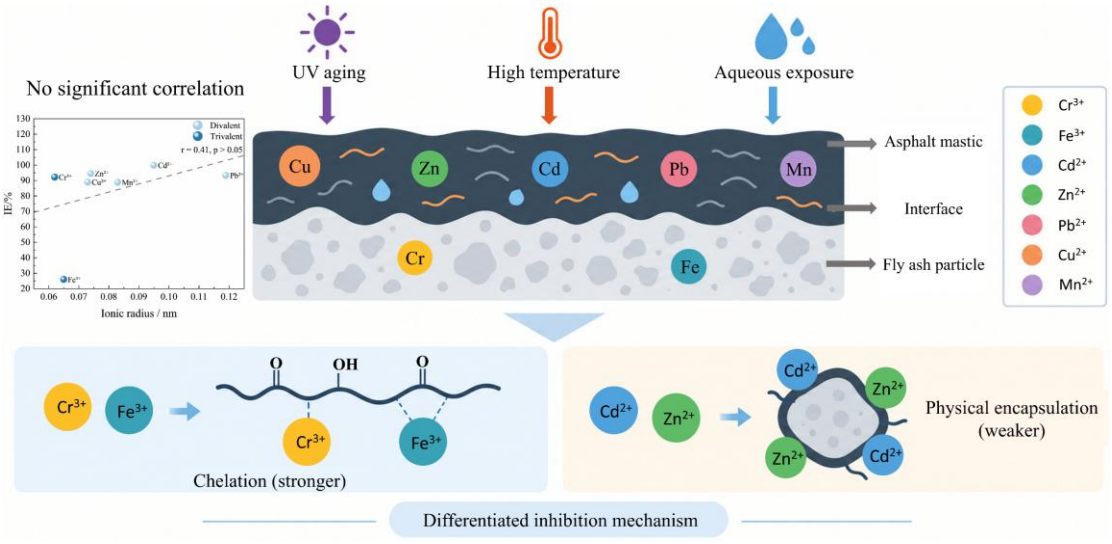


Fig. 14 Schematic mechanism of element-selective immobilization

Conclusions

The migration risk of the seven heavy metals in MSWI fly ash was not determined by total content but dominated by occurrence chemical form. Cd and Zn were dominated by the acid-soluble fraction, with the highest potential migration activity; Fe was dominated by reducible and residual fractions, with

the strongest intrinsic stability; Cr, Pb, Cu, and Mn showed mixed transitional characteristics. Occurrence form analysis can serve as a preliminary screening basis for environmental risk prediction of fly ash recycling.

The immobilization efficiency of asphalt mastic for the seven heavy metals showed significant element selectivity, with the order Cd (99.8%) > Zn (94.4%) > Pb (93.2%) > Cr (92.1%) > Cu (88.8%) > Mn (88.7%) > Fe (25.8%). The relatively low immobilization efficiency of Fe was not due to insufficient immobilization capacity of asphalt, but because its intrinsic migration activity in fly ash was extremely low, leaving limited marginal immobilization contribution from asphalt. This element selectivity provides a quantitative foundation for the graded assessment of heavy metal pollution risks.

Under the four typical service conditions of UV aging, high-temperature, spray, and condensation, the overall environmental sensitivity order of heavy metals remained consistent: Cd > Zn > Mn > (Cu/Pb) > Cr ≈ Fe. Cd was the most sensitive element under all conditions, with the highest leaching increase under the high-temperature condition; Cr and Fe showed inhibited leaching under all conditions. Environmental factors mainly regulated leaching intensity but did not change the inherent sensitivity hierarchy among elements. This stable sensitivity hierarchy can provide a reference for the formulation of long-term environmental risk monitoring schemes for pavement projects.

The selective immobilization of heavy metals in fly ash–asphalt mastic originated from differences in chemical affinity. Ionic radius showed no significant correlation with immobilization efficiency ($r = 0.41$, $p > 0.05$), and ionic valence and charge density dominated the differences in coordination affinity. Polar functional groups such as hydroxyl, carbonyl, and sulfoxide groups generated during aging formed strong coordination complexes with trivalent cations Cr^{3+} and Fe^{3+}, constituting chemical complexation-dominated retardation; their coordination with divalent cations Cd^{2+} and Zn^{2+} was weaker, and immobilization mainly depended on physical encapsulation, constituting physical encapsulation-dominated retardation. This mechanism intrinsically explains the underlying reason for the differentiated environmental responses of different heavy metals.

The conclusions of this study were based on a single filler-binder ratio and indoor accelerated aging conditions. Future work can use surface spectroscopy techniques such as X-ray photoelectron spectroscopy (XPS) to directly verify metal–functional group coordination bonds, conduct long-term field monitoring to verify the equivalence of accelerated aging, and investigate heavy metal migration behavior under different filler-binder ratios and combined service conditions, so as to further improve

the environmental risk monitoring and assessment system for engineering applications.

Declarations

Ethical Responsibilities Statement

All authors have read, understood, and have complied as applicable with the statement on "Ethical responsibilities of Authors" as found in the Instructions for Authors.

Competing Interests

The authors declare that they have no known competing financial interests or personal relationships that could have appeared to influence the work reported in this paper.

Acknowledgements

This work was supported by the R&D Project of Guangzhou North Second Ring Transportation Technology Co., Ltd. (Grant No. BEH2025RD04); the Guangdong Basic and Applied Basic Research Foundation (Grant No. 2024A1515012242); the Guangdong Basic and Applied Basic Research Foundation (Grant No. 2026A1515011592). We would like to thank the Analysis and Test Center of Guangdong University of Technology for providing valuable support and resources in conducting the analysis essential for this research.

Authors' Contributions

Yan Wang: Conceptualization, Methodology, Investigation, Formal analysis, Data curation, Writing – original draft.

Xujia Zhou: Investigation, Data curation, Formal analysis, Visualization, Writing – original draft.

Ming Ye: Investigation, Formal analysis, Validation, Visualization, Writing – review & editing.

Yuanyu Lu: Conceptualization, Supervision, Project administration, Methodology, Writing – original draft.

Xiaolong Sun: Funding acquisition, Resources, Supervision, Writing – review & editing.

Data Availability

Data will be made available on request.

References

Ajorloo, M., Ghodrat, M., Scott, J.&Strezov, V. (2022). Heavy metals removal/stabilization from

municipal solid waste incineration fly ash: a review and recent trends. *Journal of Material Cycles and Waste Management*, 24, 1693-1717. http://10.1007/s10163-022-01459-w

Azadgoleh, M. A., Mohammadi, M. M., Ghodrati, A., Sharifi, S. S., Palizban, S. M. M., Ahmadi, A., Vahidi, E.&Ayar, P. (2022). Characterization of contaminant leaching from asphalt pavements: A critical review of measurement methods, reclaimed asphalt pavement, porous asphalt, and waste-modified asphalt mixtures. *Water Research*, 219, 24. http://10.1016/j.watres.2022.118584

Bensiradj, N. E. H., Guermi, I. N. E. H., Lemghiti, H., Bessila, S., Boussaid, L., Ouamerali, O.&Zeghdaoui, A. (2026). Electronic structure and adsorption behaviour of heavy-metal dithiocarbamate complexes on iron oxides: a DFT study toward water remediation. *Molecular Physics*, 17. http://10.1080/00268976.2026.2692964

Cao, X., Ran, H., Cui, F., Chen, Z.&Yin, W. (2025). Dynamic redox-regulation of layered Fe-Cr(III) hydroxides for heavy metals capture: Exploring sustainable utilization of Fe-Cr residues. *Separation and Purification Technology*, 356, 10. http://10.1016/j.seppur.2024.129910

Cho, B. H., Nam, B. H., An, J.&Youn, H. (2020). Municipal Solid Waste Incineration (MSWI) Ashes as Construction Materials-A Review. *Materials*, 13, 30. http://10.3390/ma13143143

Cui, B.&Wang, H. (2023). Oxidative aging mechanism of asphalt binder using experiment-derived average molecular model and ReaxFF molecular dynamics simulation. *Fuel*, 345, 14. http://10.1016/j.fuel.2023.128192

Florez, E., Jimenez-Orozco, C.&Acelas, N. (2024). Unravelling the influence of surface functional groups and surface charge on heavy metal adsorption onto carbonaceous materials: An in-depth DFT study. *Materials Today Communications*, 39, 14. http://10.1016/j.mtcomm.2024.108647

Grasseschi, D., Silva, W. C., de Souza Paiva, R., Starke, L. D.&Nascimento, A. S. (2020). Surface coordination chemistry of graphene: Understanding the coordination of single transition metal atoms. *Coordination Chemistry Reviews*, 422, 35. http://10.1016/j.ccr.2020.213469

Hazim, S., Biligiri, K. P.&Ramaiah, B. J. (2026). Assessing Moisture Susceptibility and Long-Term Leaching Behavior of Municipal Solid Waste Incineration Fly Ash-Modified Asphalt Mixtures. *Transportation Research Record*, 20. http://10.1177/03611981261459423

He, D., Hu, H., Jiao, F., Zuo, W., Liu, C., Xie, H., Dong, L.&Wang, X. (2023). Thermal separation of heavy metals from municipal solid waste incineration fly ash: A review. *Chemical Engineering Journal*, 467, 17. http://10.1016/j.cej.2023.143344

He, Y.&Kasina, M. (2023). The Sequential Extraction of Municipal Solid Waste Incineration Bottom Ash: Heavy Metals Mobility and Sustainable Application of Ashes. *Sustainability*, 15, 15. http://10.3390/su151914638

Hu, R., Xie, J., Wu, S., Yang, C.&Yang, D. (2020). Study of Toxicity Assessment of Heavy Metals from Steel Slag and Its Asphalt Mixture. *Materials*, 13, 15. http://10.3390/ma13122768

Kang, C., Lan, Y., Xu, X., Zhong, Y.&Xiong, J. (2025). Physicochemical properties, heavy metal speciation and environmental risk assessment of municipal solid waste incineration fly ash from Eastern China: a particle size-dependent investigation. *Environmental Geochemistry and Health*, 47, 19. http://10.1007/s10653-025-02870-6

Li, R., Zhang, H., Wang, F., He, Y., Huang, C., Luo, L., Dong, S., Jia, X.&Tang, M. (2022). Mass fractions, solubility, speciation and isotopic compositions of iron in coal and municipal waste fly ash. *Science of the Total Environment*, 838, 11. http://10.1016/j.scitotenv.2022.155974

Li, Y., Feng, J., Yang, F., Wu, S., Liu, Q., Bai, T., Liu, Z., Li, C., Gu, D., Chen, A.&Jin, Y. (2021). Gradient aging behaviors of asphalt aged by ultraviolet lights with various intensities. *Construction and Building Materials*, 295, 21. http://10.1016/j.conbuildmat.2021.123618

Liu, C., Chen, M., Li, F., Tao, L., Lin, J., Gao, T., Tong, H., Liu, Y., Long, S., Wu, F.&Xia, Y. (2019). Stabilization of Cd^{2+}/Cr^{3+} During Aqueous Fe(II)-Induced Recrystallization of Al-Substituted Goethite. *Soil Science Society of America Journal*, 83, 483-491. http://10.2136/sssaj2018.05.0169

Liu, M., Xu, M., Zhang, X., Zhou, J., Ma, Q.&Wu, L. (2021). Poorly crystalline Fe(II) mineral phases induced by nano zero-valent iron are responsible for Cd stabilization with different soil moisture conditions and soil types. *Ecotoxicology and Environmental Safety*, 223, 8. http://10.1016/j.ecoenv.2021.112616

Long, L., Jiang, X., Lv, G., Chen, Q., Liu, X., Chi, Y., Yan, J., Zhao, X., Kong, L.&Qiu, Q. (2022). Comparison of MSWI fly ash from grate-type and circulating fluidized bed incinerators under landfill leachate corrosion scenarios: the long-term leaching behavior and speciation of heavy metals. *Environmental Science and Pollution Research*, 29, 15057-15067. http://10.1007/s11356-021-16618-z

Lu, Y., Tian, A., Zhang, J., Tang, Y., Shi, P., Tang, Q.&Huang, Y. (2020). Physical and Chemical Properties, Pretreatment, and Recycling of Municipal Solid Waste Incineration Fly Ash and Bottom Ash for Highway Engineering: A Literature Review. *Advances in Civil Engineering*, 2020,

17. http://10.1155/2020/8886134

Mohan, B., Virender, V., Gupta, R. K., Silva, M. F. C. G., Pombeiro, A. J. L., Qiao, Y.&Yang, X. (2026). Enzyme-inspired coordination chemistry in confined and interfacial microenvironments: Insights from MOFs and MXenes. *Coordination Chemistry Reviews*, 561, 32. http://10.1016/j.ccr.2026.217926

Nag, M., Saffarzadeh, A., Nomichi, T., Shimaoka, T.&Nakayama, H. (2020). Enhanced Pb and Zn stabilization in municipal solid waste incineration fly ash using waste fishbone hydroxyapatite. *Waste Management*, 118, 281-290. http://10.1016/j.wasman.2020.08.026

Nan, Y., Wang, W., Chen, H., Guo, J., Chen, Y.&Du Yuan. (2026). A Review of Research on the Valorization and Risk Management of Municipal Solid Waste Incineration Bottom Ash. *Materials*, 19, 27. http://10.3390/ma19071471

Pandey, S. K.&Bhattacharya, T. (2019). Mobility, Ecological risk and change in surface morphology during sequential chemical extraction of heavy metals in fly ash: A case study. *Environmental Technology & Innovation*, 13, 373-382. http://10.1016/j.eti.2016.10.004

Qu, Y., Luo, C., He, S., Zhang, Y.&Zhou, W. (2026). Effects of different pyrolysis conditions on chemical speciation transformation and immobilization of heavy metals in sludge. *Environmental Technology*, 47, 2928-2940. http://10.1080/09593330.2026.2708215

Song, C., Yuan, Q., Zhang, Y., Wang, J., Wang, T.&Liu, J. (2024). Study on the physical encapsulation mechanism of heavy metals in fly ash carbonation solidification based on synthetic pellets. *Fuel*, 362, 10. http://10.1016/j.fuel.2024.130856

Su, P., Xia, M., Chen, K., Wang, H., Li, X., Zhou, Z., Zhang, R., Zhang, L.&Zhao, S. (2025). Study on the Solidification/Stabilization of MSWI Fly Ash by Composite Alkali-Activated Cementitious Materials. *ACS Omega*, 10, 5659-5667. http://10.1021/acsomega.4c08962

Sun, X., Huang, G., Qin, X., He, M.&Liu, Z. (2026b). Study on the occurrence state and leaching behavior characteristics of heavy metals in municipal solid waste fly ash using asphalt-based retention medium. *Construction and Building Materials*, 541, 23. http://10.1016/j.conbuildmat.2026.147916

Sun, X., Ou, Z., Xu, Q., Qin, X., Guo, Y., Lin, J.&Yuan, J. (2023b). Feasibility analysis of resource application of waste incineration fly ash in asphalt pavement materials. *Environmental Science and Pollution Research*, 30, 5242-5257. http://10.1007/s11356-022-22485-z

Sun, X., Ou, Z., Zhao, T., Qin, X., Jin, J., Yu, H.&Li, L. (2023a). Interaction state and element leaching of waste incineration fly ash-asphalt mortar based on fillerization. *Construction and Building Materials*, 398, 17. http://10.1016/j.conbuildmat.2023.132463

Sun, X., Su, Z.&Qin, X. (2025a). Development and Potential Analysis in Resource Utilization of Municipal Solid Waste Incineration Fly Ash as Construction and Pavement Materials. *International Journal of Pavement Research and Technology*, 34. http://10.1007/s42947-025-00652-y

Sun, X., Xu, H., Qin, X., Zhu, Y.&Jin, J. (2025b). Cross-scale study on the interaction behaviour of municipal solid waste incineration fly ash-asphalt mortar: a macro-micro approach. *International Journal of Pavement Engineering*, 26, 24. http://10.1080/10298436.2025.2469114

Sun, X., Ye, Y., Qin, X., Liu, Z., Zhao, W.&Wang, Z. (2026a). Deterioration behavior and mechanism of heavy metal leaching inhibition efficiency of MSWI fly ash - asphalt mastic under ultraviolet irradiation. *Waste Management*, 215, 14. http://10.1016/j.wasman.2026.115428

Sun, X., Zhang, Y., He, M., Qin, X., Liu, Z.&Guo, Y. (2026c). Study on pollution inhibition behavior of municipal solid waste incineration fly ash-asphalt mastic based on component carriers. *Construction and Building Materials*, 537, 22. http://10.1016/j.conbuildmat.2026.147085

Wang, C., Tian, X. G., Wang, Y.&Li, G. (2024b). Asphalt aging and its anti-aging mechanism based on quantum chemistry. *Case Studies in Construction Materials*, 20, 14. http://10.1016/j.cscm.2023.e02802

Wang, C., Tian, X., Wang, Y.&Li, G. (2024c). The aging mechanism of asphalt aromatics based on density functional theory, Frontier Orbitals, IR, SARA, and GPC. *Journal of Molecular Liquids*, 396, 12. http://10.1016/j.molliq.2024.124010

Wang, H., Wu, J., Liu, Q., Wu, Y., Jing, C.&Zhu, J. (2024a). Properties deterioration of recovered bitumen under coupling multi-environment factors based on the ageing simulation device. *Road Materials and Pavement Design*, 25, 1980-2000. http://10.1080/14680629.2023.2294464

Wekpe, V. O., Whitworth, M.&Baily, B. (2024). Terrestrial environmental sensitivity index mapping (TESIM) of the coastal areas of the Niger Delta region of Nigeria. *Scientific African*, 24, 18. http://10.1016/j.sciaf.2024.e02152

Wu, J., Wu, X., Wang, J., Wang, T., Zhang, Y.&Pan, W. (2020). Speciation analysis of Hg, As, Pb, Cd, and Cr in fly ash at different ESP's hoppers. *Fuel*, 280, 11. http://10.1016/j.fuel.2020.118688

754 Xi, H., Hu, S., Zheng, Y.&Fu, S. (2026). Macro-Micro Aging Mechanisms and Correlation Analysis of
755 Asphalt Under Light-Heat-Oxygen Coupling Action. *Materials*, 19, 18.
756 http://10.3390/ma19142966
757 Xia, X., Wang, J., Hu, Y., Liu, J., Darma, A. I., Jin, L., Han, H., He, C.&Yang, J. (2022). Molecular
758 Insights into Roles of Dissolved Organic Matter in Cr(III) Immobilization by Coprecipitation with
759 Fe(III) Probed by STXM-Ptychography and XANES Spectroscopy. *Environmental Science &*
760 *Technology*, 56, 2432-2442. http://10.1021/acs.est.1c07528
761 Xu, L., Du, Y., Bruno, S., Loprencipe, G.&Moretti, L. (2024a). Viscoelastic Characteristics and
762 Mechanical Performances of Asphalt Mastic and Mixtures with Fly Ash from Municipal Solid
763 Waste Incineration Residues. *Buildings*, 14, 17. http://10.3390/buildings14030672
764 Xu, S., Cai, S., Huang, R., Xu, K., Ma, Z., Fang, L.&Zhang, C. (2024c). Investigation of aging behaviors
765 of asphalt under the coupling conditions of salt and water. *Fuel*, 365, 11.
766 http://10.1016/j.fuel.2024.131191
767 Xu, Y., Niu, K., Zhu, H., Chen, R., Ou, L.&Wang, J. (2024b). Generation and evolution mechanisms of
768 asphalt aging under the combined effects of intense UV radiation and large temperature variations.
769 *Construction and Building Materials*, 438, 13. http://10.1016/j.conbuildmat.2024.136786
770 Xue, Y., Wei, X., Zhao, H., Wang, T.&Xiao, Y. (2020). Interaction of spent FCC catalyst and asphalt
771 binder: Rheological properties, emission of VOCs and immobilization of metals. *Journal of*
772 *Cleaner Production*, 259, 8. http://10.1016/j.jclepro.2020.120830
773 Yan, K., Li, L., Zheng, K.&Ge, D. (2019). Research on properties of bitumen mortar containing
774 municipal solid waste incineration fly ash. *Construction and Building Materials*, 218, 657-666.
775 http://10.1016/j.conbuildmat.2019.05.151
776 Yang, B., Li, H., Sun, Y., Zhang, H., Liu, J., Yang, J.&Zhang, X. (2023). Chemo-rheological, mechanical,
777 morphology evolution and environmental impact of aged asphalt binder coupling thermal
778 oxidation, ultraviolet radiation and water. *Journal of Cleaner Production*, 388, 14.
779 http://10.1016/j.jclepro.2023.135866
780 Yang, J., Yang, Y., Li, Y., Chen, L., Zhang, J., Die, Q., Fang, Y., Pan, Y.&Huang, Q. (2018). Leaching
781 of metals from asphalt pavement incorporating municipal solid waste incineration fly ash.
782 *Environmental Science and Pollution Research*, 25, 27106-27111. http://10.1007/s11356-018-
783 2472-6

784 Zhang, Z., Cai, W., Hu, Y., Yang, K., Zheng, Y., Fang, C., Ma, C.&Tan, Y. (2022). Ecological Risk
785 Assessment and Influencing Factors of Heavy-Metal Leaching From Coal-Based Solid Waste Fly
786 Ash. *Frontiers in Chemistry*, 10, 12. http://10.3389/fchem.2022.932133
787 Zhang, Z., Yu, Y., Rao, Y., Wang, Y., Yu, C., Luo, Z., Zhao, H., Saffarzadeh, A., Wang, X., Wu,
788 C.&Wang, Q. (2024). Stabilization of heavy metals in municipal solid waste incineration fly ash
789 using organic chelating agents: Insight into risk assessment and function mechanism. *Science of*
790 *the Total Environment*, 914, 12. http://10.1016/j.scitotenv.2024.169986
791 Zhao, H., Tian, Y., Wang, R., Wang, R., Zeng, X., Yang, F., Wang, Z., Chen, M.&Shu, J. (2021).
792 Seasonal Variation of the Mobility and Toxicity of Metals in Beijing's Municipal Solid Waste
793 Incineration Fly Ash. *Sustainability*, 13, 13. http://10.3390/su13126532
794 Zhao, K., Hu, Y., Wang, Y., Chen, D.&Feng, Y. (2019). Speciation and Risk Assessment of Heavy
795 Metals in Municipal Solid Waste Incineration Fly Ash during Thermal Processing. *Energy &*
796 *Fuels*, 33, 10066-10077. http://10.1021/acs.energyfuels.9b02187
797 Zhao, W., Geng, J., Niu, Y., Li, X., Chen, M., Xia, C.&Zhao, S. (2023a). Aging effect of damp-heat and
798 saline-alkali environment on fatigue performance and chemical evolution of asphalt.
799 *International Journal of Pavement Engineering*, 24, 16. http://10.1080/10298436.2023.2270556
800 Zhao, Y.&Zhu, Y. (2019). Metals Leaching in Permeable Asphalt Pavement with Municipal Solid Waste
801 Ash Aggregate. *Water*, 11, 16. http://10.3390/w11102186
802 Zhao, Y., Moore, O. W., Xiao, K., Otero-Farina, A., Banwart, S. A., Wu, F.&Peacock, C. L. (2023b).
803 Behavior and Fate of Chromium and Carbon during Fe(II)-Induced Transformation of
804 Ferrihydrite Organominerals. *Environmental Science & Technology*, 57, 17501-17510.
805 http://10.1021/acs.est.3c05487
806 Zhong, Z., Xu, S., Liang, S., Wang, X., Hu, Y., Pipintakos, G., Ren, S., Liu, Q.&Wu, S. (2026). Effects
807 of Zinc Diethyldithiocarbamate (ZDC) on Rheological Behavior and Aging Resistance of SBS-
808 Modified Asphalt. *Materials*, 19, 16. http://10.3390/ma19132893
809 Zhou, X., Chen, M., Wu, S., Zhou, X., Li, L.&Ma, Z. (2024). Heavy metals and PAHs adsorption
810 characteristics of bio-asphalt in road runoff. *Journal of Cleaner Production*, 450, 11.
811 http://10.1016/j.jclepro.2024.141923
812 Zou, F., Leng, Z., Li, D., Zhang, S., Yaphary, Y. L.&Lu, G. (2023). Leaching potential of metals and
813 PAHs of asphalt rubber paving materials. *Transportation Research Part D-Transport and*

Environment, 125, 12. http://10.1016/j.trd.2023.103984

Zou, F., Leng, Z., Lu, G.&Lv, S. (2024). Leaching characteristics of metals and Polycyclic Aromatic Hydrocarbons (PAHs) from asphalt paving materials. *Science of the Total Environment*, 918, 9. http://10.1016/j.scitotenv.2024.170733

Zou, Y., Pang, L., Xu, S., Wu, S., Yuan, M., Amirkhanian, S., Xu, H., Lv, Y.&Gao, X. (2022). Investigation of the Rheological Properties and Chemical Structure of Asphalt under Multiple Aging Conditions of Heat, UV and Aqueous Solution. *Materials*, 15, 18. http://10.3390/ma15165711